Progressive ataxia, myoclonic epilepsy and cerebellar apoptosis in cystatin B-deficient mice

Len A. Pennacchio[1,2], Donna M. Bouley[3], Kay M. Higgins[4,5], Matthew P. Scott[2,4,5], Jeffrey L. Noebels[6] & Richard M. Myers[2]

Loss-of-function mutations in the gene (*CSTB*) encoding human cystatin B, a widely expressed cysteine protease inhibitor, are responsible for a severe neurological disorder known as Unverricht-Lundborg disease (EPM1). The primary cellular events and mechanisms underlying the disease are unknown. We found that mice lacking cystatin B develop myoclonic seizures and ataxia, similar to symptoms seen in the human disease. The principal cytopathology appears to be a loss of cerebellar granule cells, which frequently display condensed nuclei, fragmented DNA and other cellular changes characteristic of apoptosis. This mouse model of EPM1 provides evidence that cystatin B, a non-caspase cysteine protease inhibitor, has a role in preventing cerebellar apoptosis.

Introduction

The progressive myoclonus epilepsies (PMEs) are diseases characterized by tonic-clonic seizures, myoclonic seizures and progressive neurological dysfunction, including dementia and ataxia[1]. The five major PME types are myoclonic epilepsy and ragged-red fiber disease (MERRF), Unverricht-Lundborg disease (EPM1), the neuronal ceroid lipofuscinoses (NCLs), sialidosis and Lafora disease. The genetic bases of seven PMEs have been determined[2–9]. Loss-of-function mutations have been identified in two novel genes (*CLN3* and *CLN5*) in NCL-3 and NCL-5, *CSTB* in EPM1 and genes encoding mitochondrial tRNA lysine in MERRF, a lysosomal peptidase in NCL-2, palmitoyl-protein thioesterase in NCL-1 and sialidase (neuraminidase) in sialidosis. The cellular mechanisms of pathogenesis in three of the five PMEs (Lafora disease, sialidosis and the NCLs) appear to be similar, as these mutations result in progressive formation of intracellular inclusion bodies in a wide variety of cell types[10–13]. The mechanism of pathogenesis of MERRF is also partly understood; the symptoms are due to mitochondrial oxidative phosphorylation defects resulting in the progressive destruction of tissues sensitive to decreased ATP production[14,15]. In contrast, the fifth PME, EPM1, is not associated with inclusion bodies or mitochondrial defects, and the mechanism by which the loss of cystatin B function results in the symptoms of the disease remains unknown.

EPM1 is an autosomal recessive inherited disorder that occurs worldwide, has an onset of symptoms at 6–15 years of age and is characterized by myoclonic and tonic-clonic seizures[16–19]. Patients develop progressive neurological dysfunction, including ataxia, which may occur before or after the onset of seizures. Severity is variable both between and within families, and it is estimated that patients have an average decline in IQ of 10 points per decade[16]. In addition to the lack of biochemical markers and inclusion bodies in EPM1, the pathological basis for the disease is unclear. The few autopsy studies that were performed decades ago yielded inconclusive results. In some cases, widespread neurodegenerative changes were found, whereas in others, cell death was limited to Purkinje cells in the cerebellum and may have resulted from anti-epileptic treatment[16,20,21]. As all cases were treated before neuropathological analysis, one of the goals of our study was to create an animal model of EPM1 to study the early neuropathological changes and to define the primary events in the disease.

The biochemical and cell biological properties of cystatin B provide some clues to the pathophysiology of EPM1. Cystatin B (also known as stefin B, Stfb) belongs to a large class of proteins that inhibit cysteine proteases[22,23]. Structural and functional comparisons suggest that the cystatins comprise a single evolutionary superfamily, presumably all derived from a common ancestor[24]. The 98-aa cystatin B protein is widely distributed among different cell types and tissues. Experiments *in vitro* show cystatin B to be a tightly-binding reversible inhibitor of cathepsins B, H, L and S, and the plant cysteine protease papain[25,26]. Cathepsins B, H, L and S are lysosomal proteases involved in general protein catabolism and possibly in specific proteolytic processing events[27–29]. Although these cathepsins are localized to lysosomes, cystatin B is thought to reside in the cytosol, where it probably has a role in the regulation of proteolysis. The possibility that EPM1 is caused by the lack of a cysteine protease inhibitor suggests that the symptoms of this disease are the result of excessive proteolysis, in contrast with the insufficient cleavage events that cause intracellular inclusion bodies in the three previously described PMEs (Lafora disease, sialidosis and the NCLs). We report here the generation and characterization of *Cstb*-deficient mice. Our results show that EPM1 should be classified as a primary neurodegenerative disorder that selectively targets specific mammalian cells, and that cystatin B is necessary to prevent apoptosis in cerebellar granule cells.

[1]Department of Biological Sciences, [2]Department of Genetics, [3]Department of Comparative Medicine, [4]Department of Developmental Biology, [5]Howard Hughes Medical Institute, Stanford University School of Medicine, Stanford, California 94305-5120, USA. [6]Departments of Neurology, and Molecular and Human Genetics, Baylor College of Medicine, One Baylor Plaza, Houston, Texas 77030, USA. Correspondence should be addressed to R.M.M. (e-mail: myers@shgc.stanford.edu).

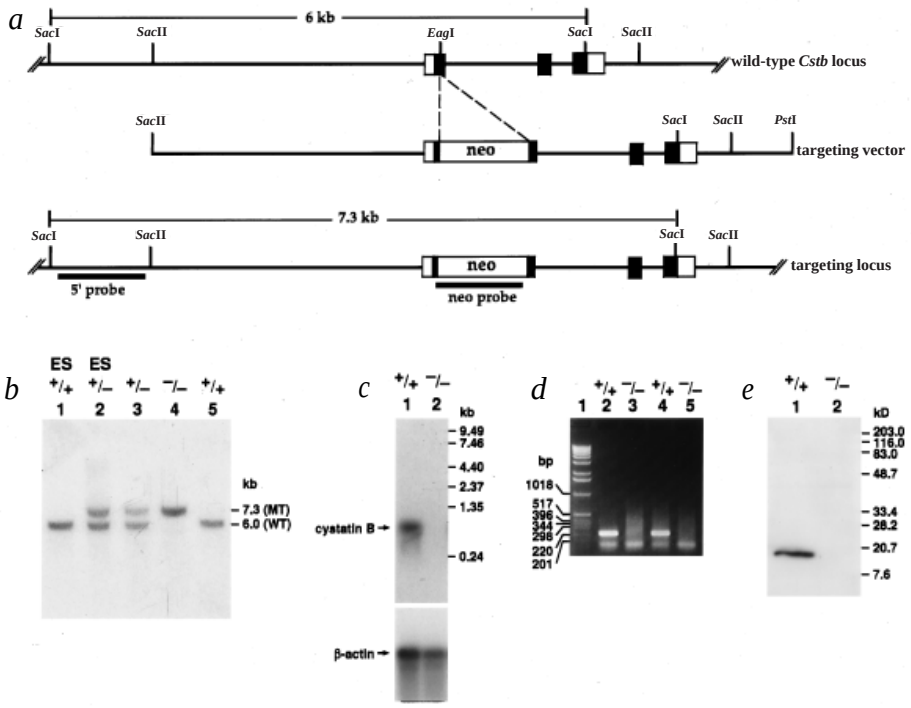

Fig. 1 Generation of *Cstb*-deficient mice. ***a***, Diagram of the *Cstb* genomic locus, the targeting vector and the predicted targeted allele. Exons are shown as boxes with the coding sequence filled in black. The targeting vector arms contain a 3.1-kb *Sac*II/*Eag*I fragment and a 2.9-kb *Eag*I/*Pst*I fragment. The PGK-neomycin cassette was inserted into the *Eag*I site in exon 1 of the gene in the sense direction. The 5' external probe used to detect targeted ES cells is indicated under the diagram. Properly targeted ES cells are predicted to contain a 1.3-kb expansion in a wild-type 6.0-kb *Sac*I allele. The location of relevant restriction sites is depicted above each diagram. ***b***, Homologous recombination results in the expansion of a 6.0-kb (WT) *Sac*I allele to 7.3 kb (MT). A Southern blot containing *Sac*I-digested DNA was probed with the 5' external probe indicated in (*a*). *Sac*I-digested ES cell DNA before the targeting event (lane 1) or after a predicted homologous recombination event (lane 2). Lanes 3–5 contain *Sac*I-digested tail DNA from three representative offspring from an intercross of mice heterozygous for the insertion. ***c***, *Cstb* transcript is absent in liver tissue from mice homozygous for the insertion. A northern blot containing total liver RNA was probed with a mouse *Cstb* cDNA probe as described[30]. The blot contains RNA from a wild-type (+/+) mouse (lane 1) and a mutant (–/–) littermate (lane 2). The location of RNA size markers is indicated to the right of the autoradiogram. A β-actin probe was hybridized to the same blot to assess the approximate quantity of RNA loaded in each lane (lower panel). ***d***, Mice homozygous for the insertion completely lack mature *Cstb* mRNA. RT-PCR was performed on wild-type (lanes 2,4; +/+) and mutant (lanes 3,5; –/–) total liver RNA and the amplified products were separated in 2.5% agarose by gel electrophoresis and visualized by ethidium bromide staining. The primers 200F1 and R100 are predicted to amplify a 225-bp product based on the *Cstb* cDNA sequence. A 1-kb DNA ladder was loaded in lane 1 as a size standard. ***e***, The cystatin B protein is absent in brain tissue from mice homozygous for the insertion. A blot containing protein extracts from brain tissues in both a wild-type (lane 1; +/+) and a mutant littermate (lane 2; –/–) were immunoprobed with an N-terminal polyclonal antibody. The location of the molecular weight marker fragments is depicted to the right of the autoradiogram.

Results

Targeted disruption of *Cstb*

We previously described the genomic organization and nucleotide sequence of mouse *Cstb* (ref. 30). To disrupt the gene, we constructed a *Cstb* targeting vector containing a 1.3-kb PGK-neomycin expression cassette inserted into the *Eag*I site in exon 1 (Fig. 1*a*). We electroporated 129Sv embryonic stem (ES) cells with linearized targeting vector and selected for neomycin gene function. Using Southern-blot analysis, six clones were identified that contained the expected 7.3-kb *Sac*I mutation fragment in addition to the 6.0-kb wild-type *Sac*I allele (Fig. 1*a*,*b*). We confirmed that the genomes of these cell lines contained single site-specific recombination events by Southern-blot hybridizations with neomycin and *Cstb*-specific probes (data not shown).

We micro-injected cells from three of six independently targeted ES cell lines into mouse C57BL/6 blastocysts, and implanted the injected blastocysts into pseudo-pregnant foster mothers. All three ES cell clones generated coat colour chimaeras with greater than 70% agouti pigmentation. Several of these males were bred to C57BL/6 females, resulting in the germline transmission of each clone. We found by Southern-blot analysis that 45% (37/82) of agouti offspring were heterozygous for the insertion. We subsequently intercrossed these heterozygous mice. Viable offspring homozygous for the insertion were produced in the expected mendelian genotype ratio of 1:2:1 (+/+:+/–:–/–, 97:204:102; Fig. 1*b*).

RNA and protein analysis

The introduction of the PGK-neomycin cassette into codon 14 of *Cstb* is predicted to cause an in-frame nonsense codon after eight additional codons, truncating the protein at 15% of its normal length. We used RNA and protein blots to test whether animals homozygous for the targeted disruption lacked cystatin B. RNA from livers of animals homozygous for *Cstb* insertion was probed with a mouse *Cstb* cDNA probe. No mature or aberrant *Cstb* RNA were detected, whereas control RNA showed the expected band at approximately 600 bases (Fig. 1*c*). We also performed RT-PCR experiments to test with greater sensitivity for mature *Cstb* mRNA. We were unable to obtain RT-PCR products from mutant RNA, whereas control RNA from wild-type littermates amplified the expected 225-bp product (Fig. 1*d*). Protein blots of brain tissue, immunoprobed with an antibody that recognizes the amino terminus of the mouse protein, identified an approximately 12-kD signal in wild-type cell extracts that was absent in mutants (Fig. 1*e*). Thus, multiple independent experimental methods indicate that mice homozygous for the targeted neomycin insertion lack cystatin B.

Development of corneal lesions in *Cstb*-deficient mice

We followed the development of *Cstb*-deficient mice through one year of age. During the three weeks before weaning, we found no visible differences in the phenotype of wild-type and mutant mice. Subsequent to weaning, at 1–3 months of age, we were unable to distinguish mutant from control mice on the basis of their size, weight, grooming behaviour, coordination and strength. We could identify approximately 40% of mutant animals because they developed an increased incidence of narrowed palpebral fissures (squinting), increased lacrimation (tearing) and periocular accumulation of serous to mucoid exudate. As the mice aged from three to seven months, 35% (23/66) of mutants and 0% (0/188) of controls developed easily discernible corneal opacity in one or both eyes (Fig. 2*a*,*b*). In 8 of 23 cases (35%), both eyes were affected.

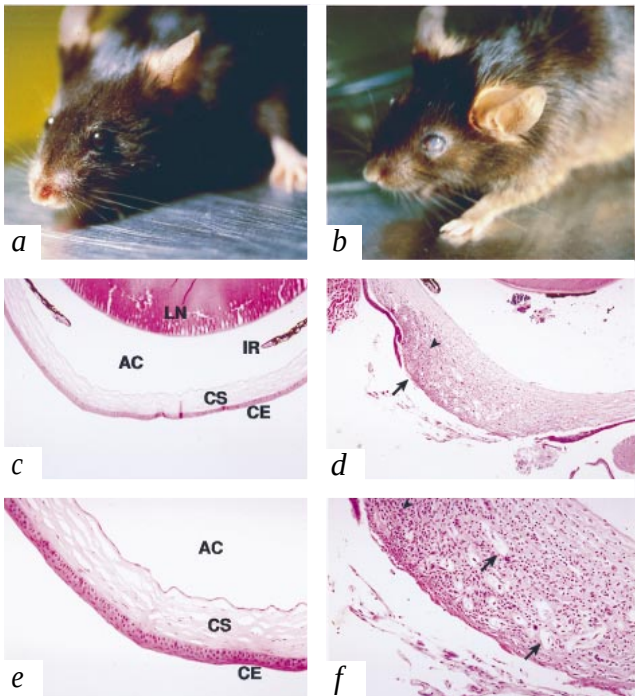

Fig. 2 *Cstb*-deficient mice develop corneal lesions. Comparison of the eyes of a control mouse (***a***) and a *Cstb*-deficient mouse (***b***) demonstrates the typical corneal opacity seen in these mice as early as three months of age. ***c***,***e***, Photomicrographs of H&E-stained longitudinal sections of eyes demonstrating the normal corneal histo-architecture from a wild-type mouse. Magnification ×10 (*c*), ×25 (*e*). AC, anterior chamber; LN, lens; IR, iris; CS, corneal stroma; CE, corneal epithelium. ***d***, Severe ulcerative keratitis representative of corneal lesions in mutant mice. Note the loss of the corneal epithelium (arrow) and the dense stromal inflammatory infiltrates (arrowhead). Magnification ×10. ***f***, Higher magnification of the affected cornea in (*d*), showing the intense inflammatory cell infiltrates (arrowhead) and numerous neocapillaries (arrows) in the corneal stroma. Magnification ×25.

To evaluate the pathological basis for the eye phenotypes, we performed complete necropsies on mutant and control mice. The macroscopic corneal opacities corresponded with histopathological lesions of acute to chronic keratitis, and a few had accompanying anterior uveitis (accumulations of neutrophils in the anterior chamber). The corneal epithelial layers were eroded, ulcerated, or hyperplastic and keratinized (Fig. 2*d*). The corneal stromas were markedly thickened and infiltrated by numerous inflammatory cells, neocapillaries and fibroblasts (Fig. 2*f*). Gram stains for bacteria and silver stains for fungi failed to reveal the presence of either pathogen; their presence would have provided an infectious aetiology for the lesions. Thus, the loss of *Cstb* leads to an increased incidence of corneal inflammation.

Development of ataxia in *Cstb*-deficient mice

We found that approximately six-month-old mutant mice showed mild signs of ataxia when challenged to walk on uneven surfaces. As the mice aged, animals walked with a wide-based gait and, upon hindlimb rearing, occasionally fell on their sides. We found no differences, however, between the swimming ability of mutants compared with controls. We compared the performance of mutant mice on the rotorod, a device that allows the quantitation of coordination, with controls in two age groups (3–4 months and 7–9 months of age; Fig. 3). We found no difference in the still or rotating rotorod performance in 3–4-month-old mutant mice compared with controls (Fig. 3*a*,*b*; n=18 for +/x; n=17 for –/–; student T-test $P>0.05$ for each comparison at each of the five trials). In contrast, mutant mice 7–9 months of age performed significantly worse than littermate controls on both the still and rotating rotorod (Fig. 3*c*,*d*; n=32 for +/x; n=33 for –/–; student T-test $P<0.0001$ for each comparison at each of the five trials).

Cerebellar granule cell loss in *Cstb*-deficient mice

We compared the gross morphology and histology between tissues lacking cystatin B and control tissues in mice at six and nine months of age. No differences were found in most tissues, although we found a depletion of granule cells in the cerebellum of $Cstb^{-/-}$ mice. The histology of brain tissue from 25 mutant and 18 control animals of 1–12 months of age was examined. The oldest mutants had a reduction in the density of the granule cell layer in the cerebellum compared with age-matched controls (Fig. 4*a*,*b*). In addition to the decreased cell density, at higher magnification numerous condensed nuclei not present in controls were seen in the granule cell layer of mutant cerebellum (Fig. 4*c*,*d*). On further examination, we found that all mutant animals contained pyknotic nuclei in the granule cell layer of the cerebellum, regardless of their age.

To assess whether these pyknotic nuclei have fragmented DNA characteristic of apoptosis, we performed terminal deoxynu-

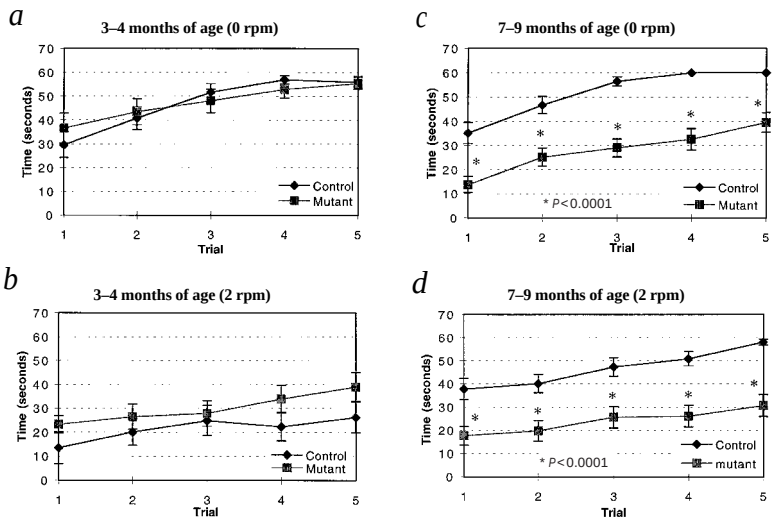

Fig. 3 Seven-to-nine-month-old mice lacking *Cstb* have impaired abilities on both the still and rotating rotorod. *a*,*b*, A summary of rotorod experiments performed on 3–4-month-old mice. Comparison (***a***) of the average performance of controls and mutants on a still (0 rpm) rod, and (***b***) the same group of mice on a rotating (2 rpm) rod. Each mouse was given five consecutive trials at 0 rpm, followed immediately by five consecutive trials at 2 rpm. Mice reaching the 60 s time point received a perfect score and were removed from the rod and immediately tested in the next trial. Error bars correspond to the standard error of the mean (n=18 for +/x; n=17 for –/–; student T-test $P>0.05$ for each comparison at each of the five trials). *c*,*d*, A summary of rotorod experiments performed on 7–9-month-old mice. Comparison (***c***) of the average performance of controls and mutants on a still (0 rpm) rod, and comparison (***d***) of the same cohort on a rotating (2 rpm) rod. The testing sequence was identical to that described above (n=32 for +/x; n=33 for –/–; student T-test $P<0.001$ for each comparison at each of the five trials). We found that 97% (31/32) and 88% (29/32) of controls and 58% (19/33) and 42% (14/33) of mutants at 7–9 months of age were able to reach the 60 s target successfully in one of their five trials at 0 and 2 rpm, respectively (data not shown).

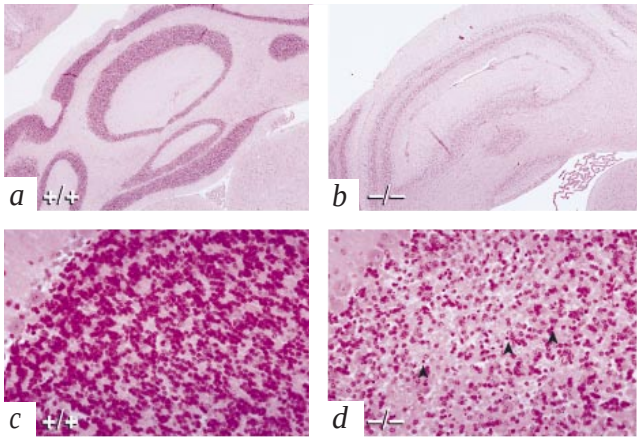

Fig. 4 *Cstb*-deficient mice have reduced cell density and contain pyknotic nuclei in the granule cell layer of the cerebellum. H&E-stained coronal sections (5 μm) of cerebellum in an 11-month-old control (***a***) and mutant (***b***); ×5 magnification. A higher magnification of H&E-stained granule cells in an 11-month-old control (***c***) and mutant (***d***); ×50 magnification. Arrowheads in (*d*) indicate several of the dark staining condensed nuclei.

cleotidyl transferase-mediated dUTP nick-end labelling (TUNEL) on brain sections[31]. We found widespread TUNEL-positive staining only in the cerebellum of all 25 mutants examined, ranging from 1–12 months of age. This staining was absent in all 18 controls (Fig. 5*a*,*c*). The vast majority of these cells were found in the granule cell layer of the cerebellum, with an occasional TUNEL-positive cell in the molecular layer (Fig. 5*c*). We counted the number of TUNEL-positive cells in the cerebellum of 2–4-month and 10–11-month-old mice (Table 1). At both ages, mutant animals had significantly more TUNEL-positive cells compared with controls (Table 1; n=5 for each group at 2–4 months of age and n=14 for each group at 10–11 months of age; student T-test $P<0.001$ when comparing mutants and controls at both age groups). At higher magnification, counterstaining with bis-benzimide, a nucleic acid stain, revealed that approximately two-thirds of TUNEL-positive cells also had condensed and irregularly-shaped nuclei, further suggesting an apoptotic mechanism of cell death (Table 1 and Fig. 5*e*,*f*).

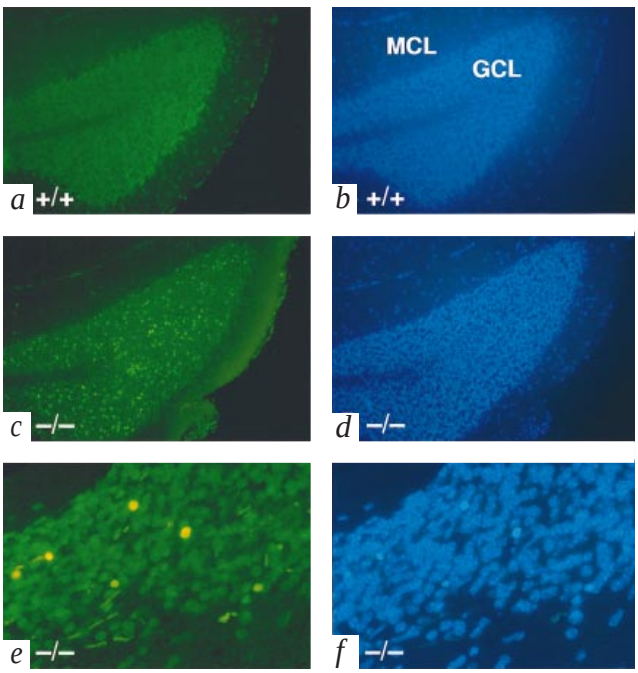

Fig. 5 *Cstb*-deficient mice display TUNEL-positive cells with condensed nuclei in the cerebellum. TUNEL (***a***) and bis-benzimide (***b***) staining in a coronal section of cerebellum from a three-month-old control mouse. TUNEL staining was visualized with a standard fluorescein filter set and bis-benzimide counterstaining with a ultraviolet filter set; magnification ×25. GCL, granule cell layer; MCL, molecular cell layer. TUNEL (***c***) and bis-benzimide (***d***) staining in a coronal section of cerebellum from a three-month-old mutant mouse. TUNEL and bis-benzimide staining were detected as described in (*a*,*b*); magnification ×25. *e*,*f*, A higher magnification of (*c*) and (*d*). TUNEL-positive cells in mutant animals (***e***) also display condensed and irregular-shaped nuclei (***f***), as determined by bis-benzimide counterstaining; magnification ×100.

The experiments described above were performed using mice containing a mixed C57BL/6 and 129Sv genetic background (F2 offspring from a $[C57BL/6\times129Sv]_{F1}$ intercross), and stronger effects on granule cell survival were seen in inbred mouse lines. We generated several pure 129Sv lines containing the insertion by directly breeding germline-transmitting chimaeric males to 129SvJ females. In several of the oldest 129Sv strain mice (2–4 months of age), we performed TUNEL analysis on brain sections. TUNEL-positive granule cells were found in the cerebellum of mutant 129Sv mice and not in controls (n=5 for mutants and controls; student T-test $P<0.001$; Table 1). The cerebellum of 129Sv mutant mice contained approximately twofold more TUNEL-positive granule cells than age-matched mutants derived from the mixed C57BL/6 and 129Sv genetic background (Table 1; $P<0.01$).

To further test whether the pyknotic cells and TUNEL results were due to apoptotic cell death, cerebellar tissue from pure 129Sv background *Cstb*-deficient mice was examined by transmission electron microscopy (TEM). We found numerous cells displaying characteristic features of apoptosis in the granule cell layer of the cerebellum in three-month-old *Cstb*-deficient mice (Fig. 6). We observed granule cells with both early apoptotic cellular features, including chromatin marginization and nuclear condensation, and late apoptotic cellular features, including the presence of apoptotic bodies and cytoplasmic vacuoles (Fig. 6). Together, the TUNEL reactivity, nuclear condensation and electron microscopy results support an apoptotic mechanism of cerebellar granule cell loss in *Cstb*-deficient mice.

Myoclonic seizures in isogenic 129Sv mutants

In addition to observing increased TUNEL-positive cells in mice lacking *Cstb* in a pure 129Sv genetic background, we found that these isogenic animals developed myoclonus and seizures during sleep by one month of age. Initially, the seizure episodes were marked by brief twitching of either the whiskers, ears or tail, followed by facial spasms and minor shaking of the torso and limbs. Subsequently, shaking became more pronounced with intermittent lightning-like muscle jerks, sometimes propelling the animal forward. Each event lasted from a few seconds to several minutes,

Table 1 • Quantitation of TUNEL in *Cstb*-deficient mice

	Average number of TUNEL-positive cells		Average number of condensed nuclei	
Age (months)	Control	Mutant	Control	Mutant
2–4	0.0±0.0	38.0±9.3*	0.0±0.1	25.0±6.2*
2–4 (129Sv)	0.1±0.1	76.8±10.3	0.1±0.1	46.7±6.3
10–11	0.0±0.1	8.2±1.1	0.0±0.0	6.3±0.7

Five fields of view at ×40 magnification were counted independently for TUNEL-positive cells and cells with condensed nuclei in the granule cell layer of the cerebellum for each mouse. 10–11-month age group +/x, n=8, –/–, n=14; 2–4-month age group +/x, n=5, –/–, n=5; 2–4-month isogenic age group +/x, n=5, –/–, n=6. *Student T-test $P<0.001$. A significant difference was also found between the 2–4-month and 10–11-month-old mutants, with the younger age group having slightly more TUNEL-positive cells (student T-test $P<0.05$).

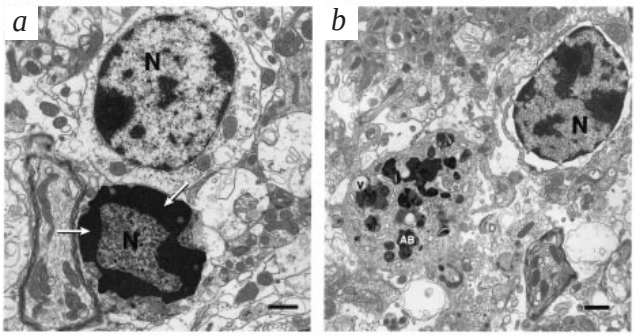

Fig. 6 Cerebellar granule cells from *Cstb*-deficient mice display cellular changes characteristic of apoptosis. ***a***, Electron micrograph of an early apoptotic granule cell. The apoptotic cell displays marginization and condensation of chromatin (arrows). N, nucleus; scale bar, 1 μm. ***b***, Electron micrograph of a late apoptotic granule cell. AB, apoptotic bodies; V, cytoplasmic vacuoles; scale bar, 1 μm.

and usually ended with a large myoclonic outburst that powerfully catapulted the animal into the air. After the seizure, animals remained motionless for several seconds, regained mobility and the event ended. When the mutant animals were asleep, the entire myoclonic seizure occurred often, sometimes every several minutes. Seizures did not occur unless the mice were asleep, as determined by visual observation and extensive electrocortical graph (EcoG) recording.

ECoG recordings from these mutants revealed abnormal cortical activity during the stereotyped behavioural seizures. Seizure episodes were clearly evident and correlated precisely (1:1) with the multifocal myoclonic activity. During this period, a bilaterally synchronous 4–6-Hz repetitive spike discharge was present that commenced with the onset of the hyperkinetic behaviour (Fig. 7). No specific discharge complex was evident in the ECoG during the sudden generalized myoclonic movements that typically terminated the episodes. ECoG activity reverted to the normal non-spiking pattern immediately upon regaining mobility, and no photoconvulsive response was obtained by 1–45-Hz photic stimulation. The behavioural and EcoG seizures were readily detected by observers blinded to genotype. ECoG recordings from awake *Cstb*-deficient mice, or mutant mice on the mixed C57BL/6 and 129Sv genetic background, showed no identifiable cortical seizure patterns, and no behavioural seizures or myoclonus were ever observed in control mice (data not shown).

Discussion

The phenotype resulting from the loss of *Cstb* provides parallels to the human disease resulting from the same genetic lesion. *Cstb*-deficient mice are developmentally normal and fertile, but develop myoclonic seizures during sleep and mild signs of ataxia at six months of age that worsen as the animals age. This ataxic phenotype is associated with widespread granule cell loss in the cerebellum, where we have identified numerous cells exhibiting cellular features characteristic of apoptotic cell death. The effects of the lack of cystatin B on granule cells provides new insights about the pathogenesis of the disease.

***Cstb*-deficient mice as a model for EPM1.** EPM1 onset occurs at 8–14 years of age and shows a phenotypic triad consisting of myoclonic seizures, progressive neurologic decline and occasional tonic-clonic seizures. The severity of the seizures is variable and there are usually photic-induced myoclonias. The progression of the neurologic features is mild and late, and the EEG usually consists of bilateral 4–6-Hz spikes, sharp waves and 3–5 s Hz spike-wave seizures[1,17,32]. *Cstb*-deficient mice develop spontaneous myoclonus and EEG seizures associated with myoclonus, as seen in the human disease[1,16–19]. Mutant mice also develop ataxia and have extensive cerebellar granule cell loss. One hallmark feature of the progressive neurological dysfunction in EPM1 is ataxia. We observed TUNEL-positive cells in all mutants regardless of age, and a decrease in the density of the granule cell layer in the cerebellum in older mutant animals. This incremental pattern of cerebellar-specific cell loss is consistent with the progressive nature of the ataxic phenotype in mutant mice. The 129Sv strain mutant mice also develop ataxia and have significantly more TUNEL-positive granule cells in the cerebellum than age-matched mutants containing the mixed background, suggesting effects from modifier genes. Although other mouse mutants, such as weaver, staggerer and lurcher, also develop ataxia associated with cerebellar cortical cell loss, these mutants lack myoclonic seizures[33–35]. Thus, cerebellar cell death alone is insufficient as a cause for myoclonic epilepsy.

There are some differences between the human disease symptoms and those found in *Cstb*-deficient mice on the backgrounds studied. The mutant mice do not develop tonic-clonic seizures, show no photosensitivity, display seizures with myoclonus only during sleep and the spike-wave complexes reported in patients have not been observed in the mutant model. Whether these differences indicate additional contributing disease factors in humans, or reflect the differences between human and mouse biology, brain development or a background strain effect, remains to be investigated. For example, granule cells are produced during fetal stages in humans, but most mouse granule cells are produced postnatally. However, the lack of myoclonic

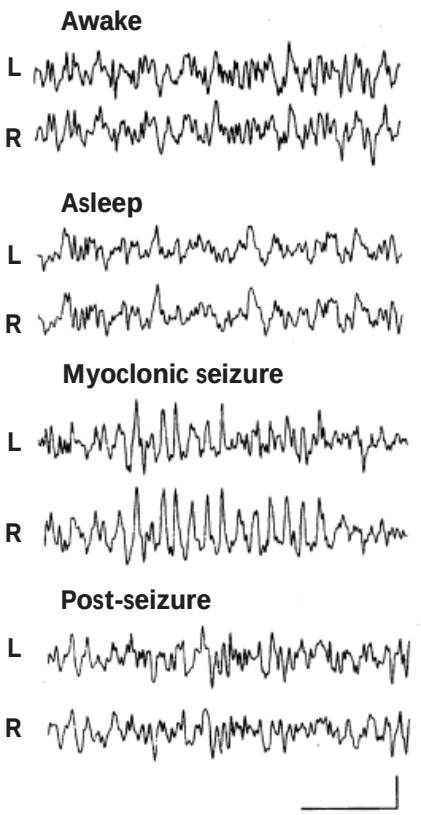

Fig. 7 *Cstb*-deficient mice develop myoclonic seizures during sleep. Electrocorticographic activity in *Cstb*-deficient mice. Traces from left and right hemispheres show spontaneous cortical activity in an adult awake and freely moving *Cstb*-deficient mutant (awake), during sleep one minute before seizure episode (asleep), during myoclonic seizure with repetitive 6–10 per second bilaterally synchronous spikes when asleep (myoclonic seizure), and immediately following the behavioural seizure episode (post-seizure). Calibration: 500 μV, 500 ms.

seizure in the mixed C57BL/6 and 129Sv genetic background compared with the *Cstb*-deficient 129Sv strain indicates that at least this phenotype is directly influenced by other genes. As mutants of the 129Sv strain were less than six months old in this study, it is possible that they will develop other elements of the phenotype found in EPM1 as they age.

Cystatin B and caspases: the block to apoptosis. How might cystatin B normally block apoptosis? Caspases are evolutionarily related cysteine proteases necessary for the execution of apoptosis. Caspases are synthesized as zymogens that are activated by limited cleavage events in a region known as the linker segment. It is possible that cystatin B normally directly inhibits caspases, so its absence results in apoptosis by allowing inappropriate caspase activity. However, although cystatin B is a cysteine protease inhibitor, there are no data to indicate that cystatin B physically interacts with the caspases. A more likely mechanism is that the cathepsins, which are inhibited by cystatin B, directly activate the caspases, thus leading to the initiation of apoptosis.

Recent studies indicate that caspase-3 is necessary for apoptosis to occur in granule neurons in the cerebellum[36,37]. Targeted gene disruption experiments indicate that the lack of caspase-3 in mice causes premature lethality associated with major morphological changes in the brain, including an increased number of cerebellar granule cells due to insufficient apoptosis during development[36]. Cultured cerebellar granule neurons also require the activation of caspase-3 to undergo apoptosis, in this case following induction by glutamate treatment[37]. These data suggest an essential role for caspase-3 in at least some forms of apoptotic cerebellar granule cell death. Although initiation of apoptosis may depend on activating caspases, it is also possible that the lack of cystatin B causes apoptosis in a more indirect manner. For example, the lack of cystatin B may cause an increase in general proteolysis that structurally damages cells and thereby leads to apoptosis of unhealthy cells.

The effect of the loss of cystatin B on apoptosis may be to activate caspases by allowing inappropriate activation of cathepsins. It was initially thought that caspases are self-activating and cleave themselves at specific aspartic acid residues in the protein, but other studies have found that non-specific proteases are capable of this activation. For instance, the serine protease cathepsin G can activate caspase-7 *in vitro* through a non-aspartic acid cleavage event. Furthermore, the intracellular loading of trypsin and chymotrypsin into various cell lines is able to initiate apoptosis, presumably by direct caspase activation[38]. These data led to the speculation[39] that the activation domain in the linker segment of caspases is especially sensitive to proteolysis, allowing the activation of caspases through non-aspartic-acid–specific cleavage events[40]. Thus, it is possible that various cathepsins are capable of cleaving caspases, especially in the absence of cystatin B, resulting in the initiation and execution of apoptosis.

Why does the loss of function of a normally ubiquitous protein, cystatin B, cause the selective neuronal loss seen in EPM1 and *Cstb*-deficient mice? One possibility is that the genetic redundancy of the cystatins protects the majority of cells from increased proteolysis, thereby targeting the vulnerable cerebellar granule cells that lack compensatory pathways. Alternatively, increased proteolytic events may be more deleterious in some cell types compared with others. The detection of apoptosis in *Cstb*-deficient mice supports the interpretation that at least some of the symptoms of EPM1 are initiated by apoptosis.

Previous neuropathological studies in EPM1 have yielded inconsistent results. In addition to the limited autopsy reports, these results are complicated by anti-epileptic drug treatments. Historically, EPM1 was treated with the common anti-convulsant drug phenytoin, until studies in the early 1980s found that this treatment increased the severity and progression of the disease in these patients[21]. Thus, questions arose about whether the neuropathology found in EPM1 was due purely to the genetic defect or to an aggravated drug response. The loss of Purkinje cells in the cerebellum in EPM1 may be due to phenytoin treatment rather than to the lack of cystatin B (ref. 21). Although Purkinje cells appeared to be spared on the genetic backgrounds studied, the granule cell loss in *Cstb*-deficient mice provides definitive evidence that the lack of this protein in the mammalian brain is sufficient to cause specific neuronal death and supports the classification of EPM1 as a primary neurodegenerative disorder.

Cystatin B function in the cornea. Whereas the ataxia and cerebellar cell loss are completely genetically penetrant, only 35% of mutant mice develop ocular opacity as a result of corneal lesions. The data indicate that the loss of cystatin B results in an increased susceptibility to corneal inflammation. Most clinical descriptions of EPM1 do not comment on ophthalmological features of the disease, although one report described visual problems and an associated clouding of the optic disc in EPM1 patients[16]. Although these ocular opacity phenotypes in mouse and human are not identical, evidence from other studies indicates important roles of proteases and their inhibitors in tears. For instance, the aqueous layer of normal tear film contains serine proteases such as plasmin, metalloproteases such as collagenase, cysteine proteases such as cathepsin B and protease inhibitors[41]. The serine protease inhibitor aprotinin has been shown to aid significantly in the healing of injured rabbit corneas, and the presence of cystatins in tear fluid suggests that they also have a role in the protection of the cornea against excessive proteolysis[42,43]. In tear fluid, increased levels of plasmin activity and/or other proteases have been detected in a variety of ocular conditions, including chemical corrosions, viral keratitis, ulceration of corneal grafts, type I acute hypersensitivity reactions, keratoconjunctivitis sicca (dry eye), as well as with the use of contact lenses[44,45]. In *Cstb*-deficient mice, the lack of the protease inhibitor in tear fluid could result in unusually high endogenous protease activity and subsequent corneal pathology. Increased proteolysis could either degrade the corneal extracellular matrix, damage the corneal epithelium directly, or alter the protective function of tear film. Such changes in the tear film could lead to a heightened sensitivity to environmental insults, such as ammonia, or increased susceptibility to potential bacterial, viral or fungal pathogens and their cysteine proteases. A minimal initial inflammatory response to such insults could escalate without the protective mechanisms found in tears that can neutralize the potentially damaging lysosomal enzymes contained in neutrophils. Mice lacking transforming growth factor α develop corneal opacity, similar to that seen in $Cstb^{-/-}$ mice, in approximately 40% of mutants and 13% of heterozygotes[46]. However, TNFα-deficient mice also have developmental ocular defects that are not present in our mutant mice, suggesting that different mechanisms underlie the pathology in these two mutant animals.

Our results implicate cystatin B in preventing apoptosis in cerebellar granule cells and imply that a similar mechanism of cell loss may occur in EPM1. Although apoptosis has not been previously studied in EPM1, neuronal apoptotic cell death has been found in the related PME Batten disease[47] (juvenile neuronal ceroid lipofuscinosis, JNCL). This result suggests that the intracellular inclusion bodies found in the NCLs, as well those in Lafora disease and sialidosis, may induce apoptosis, and thus neurodegeneration. This mechanism of apoptosis initiation is different from that found in EPM1, but results in a similar neurodegenerative consequence. One interpretation is that the timing and localization of

this neuronal apoptotic cell loss determines the particular symptoms found in each PME. The mouse model of EPM1 described in this paper supports a focus on early proteolytic events involved in controlling granule cell formation and preservation. The animals generated in this study provide a reagent for testing hypotheses regarding the roles of particular target proteases in the various symptoms of the disease, as well as their relationship to apoptosis.

Methods

Construction of the targeting vector. We previously isolated BAC clone 310P21 by screening a pooled mouse genomic BAC library (Research Genetics) by PCR with oligonucleotides designed to the *Cstb* nucleotide sequence[30]. A 6.0-kb *Sac*I fragment and a 1.6-kb *Pst*I fragment were subcloned from the BAC clone into plasmid vector pBluescript II SK$^+$ (Stratagene) to yield pBS-*Sac*I-6 and pBS-*Pst*I-1.6, respectively. Subsequently, pBS-*Pst*I-1.6 was digested with *Sac*II to remove approximately 800 bp and was replaced with a 5.2-kb *Sac*II fragment from pBS-*Sac*I-6 to create the larger pBS-*Sac*II/*Pst*I clone (Fig. 1*a*). Finally, the *Eag*I site (located in codons 13–15 in exon 1) of pBS-*Sac*II/*Pst*I was filled in with Klenow and a blunt-end filled *Eco*RI/*Bam*HI fragment containing the PGK neomycin cassette was inserted to create pBS-*Sac*II/*Pst*I-Neo.

Detection of homologous recombination in ES cells. pBS-*Sac*II/*Pst*I-Neo targeting vector (30 µg) linearized with *Not*I was electroporated into approximately 5×10^7 R1 ES cells with a Gene-Pulser (Bio-Rad Laboratories) at 500 µF and 250 V. Transfected cells were plated on five gelatinized 60 mm dishes pre-seeded with irradiated (6000 rad) mouse embryonic feeder (MEF) cells (Genome Systems). One day after plating, positive selection was performed in the presence of Geneticin (250 µg/ml; G418, Gibco). Resistant clones were picked at day nine and expanded into 24-well plates pre-seeded with irradiated MEF cells. *Sac*I-digested genomic DNA from individual clones was analysed by Southern blot with a 1-kb probe derived from genomic sequence immediately upstream of the targeting vector (Fig. 1*a*). The 1-kb fragment was generated by using PCR with the primers 220F1, 5′–AAGCCTTGAACACTGCACAGTGAT–3′ and 224R3, 5′–AAGACACAGGCAAAGCACCTCTAC–3′. The PCR conditions were as follows: an initial incubation at 94 °C for 5 min followed by 30 cycles for 30 s at 94 °C, 30 s at 60 °C, 1 min at 72 °C, with a final incubation for 10 min at 72 °C.

Generation of *Cstb*-deficient mice. Approximately 10–15 ES cells from each of three targeted clones were injected into C57BL/6 blastocysts[48]. An average of 10 injected blastocysts were transferred into pseudopregnant female recipient C57BL/6×CBA^{F1} mice. All three ES cell clones produced several chimaeras with greater than 50% agouti coat colour. The male chimaeras were bred to C57BL/6 females to allow for the detection of germline transmission by the agouti coat colour marker. Approximately one-half of agouti offspring (37 of 82) were positive for the insertion, as determined by Southern-blot analysis. Heterozygous mice were crossed to generate animals homozygous for the insertion for subsequent analyses.

RNA analysis. Total RNA was isolated from liver tissue by using the total RNA isolation system (Promega). Total RNA (approximately 10 µg) was separated in 1.6% agarose by gel electrophoresis and the RNA was transferred to a Hybond N$^+$ membrane (Amersham). The RNA blot was hybridized with a mouse *Cstb* cDNA probe as described[30]. Reverse transcription-PCR was performed with primers 200F1, 5′–CGCGCCATCGCCACAAT–3′ and R100, 5′–GGCTTGTTTTCATGAGGGAG–3′ as described by the manufacturer (M-MLV; Gibco).

Protein analysis. Liver and brain tissue were dissected from approximately four-week-old mice and extracts were prepared in ice-cold lysis buffer (1.0 ml) as described[49]. Protein extracts (100 µg) were separated in 16% SDS-polyacrylamide by gel electrophoresis[50] (PAGE). Prestained SDS-PAGE protein standards were used as molecular weight markers (BioRad Laboratories). Gels were transferred to Immobilon-P transfer membranes (Millipore). Membranes were blocked in TTBS (10 mM Tris, pH 8.0, 150 mM NaCl, 0.05% Tween 20) with 5% nonfat milk for 1 h and immunoprobed with a 1:500 dilution of a mouse cystatin B antibody in TTBS at RT overnight. The antibody was generated by immunizing rabbits with a peptide with the sequence EVADQVKSQLESKE. Affinity purification was performed using a HiTrap-NHS activated column as described by the manufacturer (Pharmacia Biotech). Three washes were performed in TTBS, followed by secondary antibody probing with a donkey anti-rabbit IgG horseradish peroxidase conjugate (Amersham). Detection was performed with the Renaissance kit (NEN Life Science Products).

Histological analysis. Whole eyes and brains, in addition to samples of internal viscera, were collected from carbon-dioxide euthanized mice, and were fixed in 10% buffered neutral formalin. Routine processing, paraffin embedding and haematoxylin and eosin staining (H&E) were performed on sections (5 µm). Four levels of longitudinal eye sections and multiple levels through the cerebral hemispheres and cerebellum were examined for each mouse. The eyes and brains were examined, in a blinded fashion, by a veterinary pathologist. TUNEL was performed as described by the manufacturer (Promega). Nuclei were stained for 15 min with bis-benzimide (1 µg/ml) in PBS. Five fields of coronal sections at ×40 were examined for each mouse and the number of TUNEL-positive cells and condensed nuclei were independently recorded.

Hybridization analysis. ES cell and mouse tail DNA was digested with *Sac*I according to the manufacturer's recommendations (New England Biolabs). Digested DNA (approximately 10 µg) was separated in 1% agarose by gel electrophoresis and transferred to Hybond N$^+$ membranes (Amersham). Membranes were baked for 2 h at 85 °C, followed by hybridization with [α-^{32}P]dATP random-primed probes. Filters were washed twice for 20 min in 0.1×SSC/0.1% SDS at 65 °C.

RNA blot hybridization was performed in 5×SSPE, 10×Denhardt's solution, salmon sperm DNA (100 µg/ml), 50% formamide and 2% SDS at 42 °C for 18 h. Filters were washed with 2×saline sodium citrate (SSC) at RT for 30 min and in 0.1×SSC/0.1% SDS at 60 °C for 30 min. All blots were exposed to film overnight with a single intensifying screen at –70 °C.

Rotorod analysis. A 3-cm diameter rotorod (IITC Life Sciences Instruments) consisting of a plastic roller flanked by two round plastic plates was used for both still and rotating experiments. Briefly, mice were placed on the still rotorod for five consecutive trials and times were recorded between their initial placement on the rod and a fall. Following five still rotorod trials, mice were immediately tested for five consecutive trials on a 2-rpm rotating rod and the time between their initial placement on the rod and a fall were recorded. Mice remaining on the rod for 60 s received a perfect score and were removed and placed back on the rod for the subsequent trial.

Electron microscopy. Brain tissues were dissected and fixed in 2% formaldehyde/0.5% glutaraldehyde in phosphate buffer (0.1 M) for 2 h at 4 °C. Sections were rinsed twice in phosphate buffer for 10 min, followed by postfixation in 1% osmium tetroxide (in 0.1 M phosphate buffer) for 1 h at RT. Subsequently, the sections were rinsed twice in distilled water for 10 min, dehydrated through an ethanol series and embedded in Epon. Ultrathin sections were cut, collected on grids and then stained with 1% aqueous uranyl acetate and lead citrate before examination with a Phillips 201c microscope.

Electrocorticographic recordings. We implanted silver wire electrodes (0.005-inch diameter) soldered to a microminiature connector bilaterally into the subdural space over frontal and parietal cortex of anesthetized mice several days before recording. Cortical activity was recorded using a digital electroencephalograph (TECA) from three mutants and controls on each genetic background moving freely in the test cage for prolonged periods, including sleep. Seizure behaviour was observed directly and annotated on all recordings.

Acknowledgements

We thank D. Cox, D. Vollrath, C. Prange Pennacchio, C. Iannicola, C. Karlovich, G. Barsh and members of the Myers laboratory for discussions and support, F. Davies for use of the rotorod, A. Nagy for the R1 ES cells donation, N. Ghouri for EM sample preparation, S. Krajewski for assistance with EM interpretations and C. Davis for his help with ECoG recordings. This work is supported by grant NIH NS29709 and HD24064 (J.L.N.).

Received 23 July; accepted 10 September 1998.

1. Berkovic, S.F., Andermann, F., Carpenter, S. & Wolfe, L.S. Progressive myoclonus epilepsies: specific causes and diagnosis. *New Eng. J. Med.* **315**, 296–305 (1985).
2. Schoffner, J.M., Lott, M.T. & Lezza, A.M.S. Myoclonus epilepsy and red-ragged fiber disease (MERRF) is associated with a mitochondrial DNA $tRNA^{lys}$ mutation. *Cell* **61**, 931–937 (1990).
3. Vesa, J. *et al.* Mutations in the palmitoyl protein thioesterase gene causing infantile neuronal ceroid lipofuscinosis. *Nature* **376**, 584–587 (1995).
4. International Batten Disease Consortium. Isolation of a novel gene underlying Batten disease, CLN3. *Cell* **82**, 949–957 (1995).
5. Bonten, E., van der Spoel, A., Fornerod, M., Grosveld, G. & d'Azzo, A. Characterization of human lysosomal neuraminidase defines the molecular basis of the metabolic storage disorder sialidosis. *Genes Dev.* **10**, 3156–3169 (1996).
6. Pennacchio, L.A. *et al.* Mutations in the gene encoding cystatin B in progressive myoclonus epilepsy (EPM1). *Science* **271**, 1731–1734 (1996).
7. Lalioti, M.D. *et al.* Identification of mutations in cystatin B, the gene responsible for the Unverricht-Lundborg type of Progressive Myoclonus Epilepsy (EPM1). *Am. J. Hum. Genet.* **60**, 342–351 (1997).
8. Sleat, D.E. *et al.* Association of mutations in a lysosomal protein with classical late-infantile neuronal ceroid lipofuscinosis. *Science* **277**, 1802–1805 (1997).
9. Savukoski, M. *et al. CLN5*, a novel gene encoding a putative transmembrane protein mutated in Finnish variant late infantile neuronal ceroid lipofuscinosis. *Nature Genet.* **19**, 286–288 (1998).
10. Harriman, D.G.F. & Millar, J.H.D. Progressive familial myoclonic epilepsy in 3 families: its clinical features and pathological basis. *Brain* **78**, 325–349 (1955).
11. Zeman, W. & Alpert, M. On the nature of the "stored" lipid substances in juvenile amaurotic idiocy (Batten-Spielmeyer-Vogt). *Ann. Histochim.* **8**, 255–257 (1963).
12. Carpenter, S., Karpati, G., Andermann, F., Jacob, J.C. & Andermann, E. Lafora's disease: peroxisomal storage in skeletal muscle. *Neurol.* **24**, 531–538 (1974).
13. O'Brien, J.S. The cherry red spot-myoclonus syndrome: a newly recognized inherited lysosomal storage disease due to acid neuraminidase deficiency. *Clin. Genet.* **14**, 55–60 (1978).
14. Wallace, D.C. *et al.* Familial mitochondrial encephalomyopathy (MERRF): genetic, pathophysiological, and biochemical characterization of a mitochondrial DNA disease. *Cell* **55**, 601–610 (1988).
15. Bindoff, L.A. *et al.* Multiple defects of the mitochondrial respiratory chain in a mitochondrial encephalopathy (MERRF): a clinical, biochemical and molecular study. *J. Neurol. Sci.* **102**, 17–24 (1991).
16. Koskiniemi, M., Donner, M., Majuri, H., Haltia, M. & Norio, R. Progressive myoclonus epilepsy: a clinical and histopathological study. *Acta Neurol. Scand.* **50**, 307–332 (1974).
17. Koskiniemi, M., Toivakka, E. & Donner, M. Progressive myoclonus epilepsy: electroencephalographical findings. *Acta Neurol. Scand.* **50**, 333–359 (1974).
18. Norio, R. & Koskiniemi, M. Progressive myoclonus epilepsy: genetic and nosological aspects with special reference to 107 Finnish patients. *Clin. Genet.* **15**, 382–398 (1979).
19. Koskiniemi, M. in *Paediatric Epilepsy* (eds Sillanpää, M., Johannessen, S.I., Blennow, G. & Dam, D.) 37–144 (Wrightson, Hampshire, 1990).
20. Haltia, M., Kristensson, K. & Sourander, P. Neuropathological studies in three Scandanavian cases of progressive myoclonus epilepsy. *Acta Neurol. Scand.* **45**, 63–77 (1969).
21. Eldridge, R., Iivanainen, M., Stern, R., Koerber, T. & Wilder, B.J. "Baltic" myoclonus epilepsy: hereditary disorder of childhood made worse by phenytoin. *Lancet* **2**, 838–842 (1983).
22. Barrett, A.J. *et al.* Nomenclature and classification of the proteins homologous with the cysteine-proteinase inhibitor chicken cystatin. *Biochem. J.* **236**, 312 (1986).
23. Turk, V. & Bode, W. The cystatins: protein inhibitors of cysteine proteinases. *FEBS Lett.* **285**, 213–219 (1991).
24. Rawlings, N.D. & Barrett, A.J. Evolution of proteins of the cystatin superfamily. *J. Mol. Evol.* **30**, 60–71 (1990).
25. Ritonja, A., Machleidt, W. & Barrett, A.J. Amino acid sequence of the intracellular cysteine proteinase inhibitor cystatin B from human liver. *Biochem. Biophys. Res. Comm.* **131**, 1187–1192 (1985).
26. Barrett, A.J. *et al.* Inhibitors of cysteine proteases. in *Proteinease Inhibitors* (eds Barrett, A.J. & Salvesen, G.) 515–569 (Elsevier Publishing, New York, 1986).
27. Barrett, A.J. & Kirschke, H. Cathepsin B, cathepsin H, and cathepsin L. in *Methods in Enzymology* Vol. 80 (ed. Lorand, L.) 535–561 (Academy Press, New York, 1981).
28. Bohley, P. & Seglen, P.O. Proteases and proteolysis in the lysosome. *Experientia* **48**, 151–157 (1992).
29. Marks, N., Berg, M.J. & Benuck, M. Preferential action of rat brain cathepsin B as a peptidyl dipeptidase converting pro-pioid oligopeptides. *Arch. Biochem. Biophys.* **249**, 489–499 (1986).
30. Pennacchio, L.A. & Myers, R.M. Isolation and characterization of the mouse cystatin B gene. *Genome Res.* **6**, 1103–1109 (1996).
31. Gavrieli, Y., Sherman, Y. & Ben-Sasson, S.A. Identification of programmed cell death in situ via specific labeling of nuclear DNA fragmentation. *J. Cell Biol.* **119**, 493–501 (1992).
32. Kyllerman. M., Sommerfelt, K., Hedstrom, A., Wennergren, G. & Holmgren, D. Clinical and neurophysiological development of Unverricht-Lundborg disease in four Swedish siblings. *Epilepsia* **32**, 900–909 (1991).
33. Sax, D.S., Hirano, A. & Shofer, R.J. Staggerer, a neurological murine mutant. An electron microscopic study of the cerebellar cortex in the adult. *Neurol.* **18**, 1093–1100 (1968).
34. Rakic, P. & Sidman, R.L. Organization of cerebellar cortex secondary to deficit of granule cells in weaver mutant mice. *J. Comp. Neurol.* **152**, 133–161 (1973).
35. Caddy, K.W.T. & Biscoe, C.H. Structural and quantitative studies on the normal C3H and lurcher mutant mouse. *Philosoph. Trans. R. Soc. London* **287**, 167–201 (1979).
36. Kuida, K. *et al.* Decreased apoptosis in the brain and premature lethality in CPP32-deficient mice. *Nature* **384**, 368–372 (1996).
37. Du, Y. *et al.* Activation of a caspase 3-related cysteine protease is required for glutamate-mediated apoptosis of cultured cerebellar granule neurons. *Proc. Natl Acad. Sci. USA* **94**, 11657–11662 (1997).
38. Williams, M.S. & Henkart, P.A. Apoptotic cell death induced by intracellular proteolysis. *J. Immunol.* **153**, 4247–4255 (1994).
39. Salvesen, G.S. & Dixit, V.M. Caspases: Intracelluar signaling by proteolysis. *Cell* **91**, 443–446 (1997).
40. Zhou, Q. & Salvesen, G.S. Activation of pro-caspase-7 by serine proteases includes a non-canonical specificity. *Biochem. J.* **324**, 361–364 (1997).
41. Tsung, P.K. & Holly, F.J. Protease activity in human tears. *Curr. Eye Res.* **1**, 351–355 (1981).
42. Barka, T., Asbell., P.A., van der Noen, H. & Prasad, A. Cystatins in human tear fluid. *Curr. Eye Res.* **10**, 25–34 (1991).
43. Cejkova, J., Lojda, Z., Salonen, E.M. & Vaheri, A. Histochemical study of alkali-burned rabbit anterior eye segment in which severe lesions were prevented by aprotinin treatment. *Histochemistry* **92**, 441–448 (1989).
44. Salonen, E.M., Tervo, T., Torma, E., Tarkkanen, A. & Vaheri, A. Plasmin in tear fluid of patients with corneal ulcers: basis for new therapy. *Acta Ophthalmol.* **65**, 3–12 (1987).
45. Tervo, T. *et al.* Contact lens wear is associated with the appearance of plasmin in the tear fluid-preliminary results. *Graefes Arch. Clin. Exp. Ophthalmol.* **227**, 42–44 (1989).
46. Luetteke, N.C. *et al.* TGFα deficiency results in hair follicle and eye abnormalities in targeted and waved-1 mice. *Cell* **73**, 263–278 (1993).
47. Lane, S.C., Jolly, R.D., Schmechel, D.E., Alroy, J. & Boustany, R.-M. Apoptosis as a mechanism of neurodegeneration in Batten's disease. *J. Neurochem.* **67**, 677–683 (1996).
48. Bradley, A. Production and analysis of chimaeric mice. in *Teratocarcinomas and Embryonic Stem Cells: A Practical Approach* (ed. Robertson, E.J.) 113–151 (IRL Press, Oxford, 1987).
49. Mangiarini, L. *et al.* Exon 1 of the HD gene with an expanded CAG repeat is sufficient to cause a progressive neurological phenotype in transgenic mice. *Cell* **87**, 493–506 (1996).
50. Laemmli, U.K. Cleavage of structural proteins during the assembly of the head of bacteriophage T4. *Nature* **227**, 680–685 (1970).